Journal of Volcanology and Geothermal Research 466 (2025) 108405

Contents lists available at ScienceDirect

Journal of Volcanology and Geothermal Research

journal homepage: www.journals.elsevier.com/journal-of-volcanology-and-geothermal-research

Magma–carbonate country rock interaction can provide H_2O during magma ascent: Results from fluid and melt inclusions in skarn xenoliths from Breccia Museo, Campi Flegrei (Southern Italy)

Annamaria Lima [a], Giovanni Macedonio [b,*], Rosario Esposito [c], Harvey E. Belkin [d]

[a] Dipartimento di Scienze della Terra dell'Ambiente e delle Risorse (DiSTAR), Università degli Studi di Napoli Federico II (Retired), Napoli 80126, Italy
[b] Istituto Nazionale di Geofisica e Vulcanologia, Osservatorio Vesuviano, 80124 Napoli, Italy
[c] Dipartimento di Scienze dell'Ambiente e della Terra, Università di Milano Bicocca, Milano 20126, Italy
[d] U.S. Geological Survey (Retired), 11142 Forest Edge Dr., Reston, VA 20190, USA

ARTICLE INFO

Keywords:
Saline carbonate melt inclusions
Magma-carbonate rock interaction
Skarn formation
Eruption explosivity
Melt immiscibility
Campi Flegrei

ABSTRACT

In this paper, the results of a study on fluid inclusions (FIs) and melt inclusions (MIs) hosted in skarn-bearing minerals sampled in the Breccia Museo deposits at Campi Flegrei (Southern Italy) are reported and discussed to investigate magma-carbonate interactions. The Campi Flegrei shallow magma chamber fluid environment has been interpreted as similar to that documented in the magmatic-hydrothermal systems associated with porphyry copper deposits. Skarns form along the top and sides of the magma chamber in the brittle-plastic transition zone, where magmatic fluids accumulate through magmatic vesiculation and magma interacts with carbonate country rocks. Melt inclusions, here named saline-carbonate-melt inclusions (SCMI), trapped in olivine, provide crucial insights into the melt that forms in this setting. Heating/cooling experiments on SCMI show that they trapped a homogeneous melt that, on cooling, undergoes instantaneous unmixing, leading to the formation of three immiscible liquids: silicate, carbonate and hydrosaline (brine). The melt behavior on micrometer scales, in SCMI, is assumed reproduces what happens on a large scale, this means that in the transition zone melt remains homogeneous at $T > 980$ °C and instantly unmixes when cooled below 790 °C. To account for the instant unmixing and the absence of CO_2 in SCMI shrinkage bubbles, we propose that at high T the reaction of $CaCO_3$ with H_2O (by magma second boiling) produces $Ca(OH)_2$ and H_2CO_3 that dissolve in the homogeneous melt and prevent the formation of CO_2. At lower T by unmixing, $CaCO_3$ re-forms, releasing H_2O. The carbonate plays an essential role as it removes at high T, one mole of CO_2 from homogeneous melt and simultaneously releases two moles of H_2O at lower T when unmixing occurs. We argue that, during magma ascent, this water supply can facilitate the upward propagation of dyke to the surface and can enhance explosivity, during an ongoing eruption.

1. Introduction

Many volcanoes hosted in carbonate sequences, as the Campi Flegrei (CF) volcanic system, produce explosive eruptions. There are still unresolved questions on the interaction of magma-carbonate country rocks, whether their interaction can trigger or increase the explosiveness of the eruption and what is the role of CO_2 that forms through the carbonate melting (Deegan et al., 2010; Sottili et al., 2010; Freda et al., 2011; Troll et al., 2012; Jolis et al., 2015; Blythe et al., 2015; Knuever et al., 2023b; Iacono-Marziano et al., 2009; Esposito et al., 2023). The CF volcanic system has been interpreted as a porphyry-copper system in its embryonic state because the fluid environment of its shallow magma chamber is similar to that documented for these systems (Fedele et al., 2006; Bodnar et al., 2007; Belkin and De Vivo, 2023; Belkin et al., 2024; Lima et al., 2009, 2021, 2025). Porphyry copper systems are associated with arc volcanism and tectonic variations act as a trigger for their formation (Sillitoe, 2010). Fig. 3 shows a schematic cross section through a hypothetical granodiorite porphyry copper system in development (Burnham, 1979). Magma may erupt volcanic rocks, but generally prior to initiation of the systems because when magmatic activity weakens it evolves as a porphyry copper- type system and magma chamber get deeper and deeper (compare Fig. 3A and C). Episodic decompression take place when fluids in lithostatic pressure regime push until the crystalline shell fractures producing brecciation, dykes

* Corresponding author at: Istituto Nazionale di Geofisica e Vulcanologia, Osservatorio Vesuviano, Via Diocleziano 328, 80124 Napoli, Italy.
E-mail address: giovanni.macedonio@ingv.it (G. Macedonio).

https://doi.org/10.1016/j.jvolgeores.2025.108405
Received 25 March 2025; Received in revised form 13 June 2025; Accepted 28 June 2025
Available online 30 June 2025

and ore depositions in veins and fractures (Fig. 3B and C). Skarns form along the top and sides of the magma chamber in the brittle-plastic transition zone between the magma dominated system and the hydrothermal dominated systems, where numerous chemical reactions occur. Fluid inclusions (FIs) and melt inclusions (MIs) preserved in skarn minerals can provide useful information on the chemical-physical conditions of the transition zone and on carbonate country rock interaction.

This study reports the results of an investigation on FIs hosted in sanidine and on Mis, here named saline-carbonate-melt inclusions (SCMI), hosted in olivine crystals from a skarn xenolith, of about 70 cm large, sampled in the lithic-rich Breccia Unit (BU) of the Breccia Museo (BM) deposits cropping out at Punta della Lingua, Procida island (Fig. 1A-C). Certainly, the skarn formed before the CI eruption and likely by carbonate country rock interaction with CI magma residing in the shallow magma chamber for a long repose time before erupting.

BM belongs to the Campanian Ignimbrite (CI), one of the most explosive eruptions of the Mediterranean area in the last 200 ka (Rolandi et al., 2020a).

This paper aims to shed light on the role that carbonate might have in magma triggering explosive eruptions and, possibly, to propose a new vision of the processes that might favor an explosive eruption.

2. Geological background

2.1. The Campi Flegrei Volcanic Field

The CF volcanic field in Southern Italy is the largest Quaternary volcanic complex in the Campanian Region (Fig. 1A and B). Currently, CF is the area at the highest risk within the densely inhabited Neapolitan volcanic area because it is actively experiencing the phenomenon of bradyseism (slow ground uplift and subsidence; Lima et al., 2021 and Lima et al., 2025). It is part of the Plio-Quaternary Campanian magmatism associated with NW-SE and NE-SW trending normal faults that reflect the extensional/transtensional tectonic regime of the Campanian margin (e.g. Milia, 2010; Milia and Torrente, 2011, 2020; Peccerillo, 2017; Esposito et al., 2018; Esposito, 2020). The CF district features a ~ 12 km wide caldera depression, whose formation has been debated. Some researchers (e.g. Orsi et al., 2004; Perrotta et al., 2006) interpreted it as a nested and resurgent caldera formed by two eruptions: the CI occurring at ~40 ka (Giaccio et al., 2017), and the Neapolitan Yellow Tuff eruption (NYT), dated at ~15 ka (Deino et al., 2004). Other researchers (De Vivo et al., 2010; De Vivo et al., 2001; Rolandi et al., 2003, 2020a, 2020b) proposed that the CI had instead erupted from multiple fissures that occurred along faults associated with the local extensional tectonic regime. Recently, a "hybrid" model has been elaborated (Orsi, 2022), in which the CI originates from vents within the CF caldera and through faults. CI eruption started with a Plinian column that dispersed ash and lapilli to the East and South (e.g. Scarpati and Perrotta, 2016). Successively, pyroclastic density currents (PDCs) deposited the main CI sequence (i.e. at proximal and medial exposures; Fedele et al., 2008, 2016; Scarpati et al., 2020), and generated co-ignimbrite tephra plumes that travelled over large distances in the central and eastern Mediterranean region and even up to eastern Europe and western Asia (e.g., Pyle et al., 2006; Anikovich et al., 2007; Lowe et al., 2012; Nowaczyk et al., 2012; Giaccio et al., 2017; Petrosino et al., 2019). Estimates for the total volume of erupted magma are very variable, with values that range between 49 and 300 km^3 DRE (dense rock equivalent; Fedele et al., 2007; Rolandi et al., 2020b; Silleni et al., 2020; Scarpati et al., 2014). Recently there seems to be more consensus around the higher value given the wide diffusion of products ascribed to the IC eruption.

In proximal exposures, the CI eruption emplaced a complex formation named Breccia Museo (BM), as demonstrated by detailed geochronological, volcanological and geochemical data (Melluso et al.,

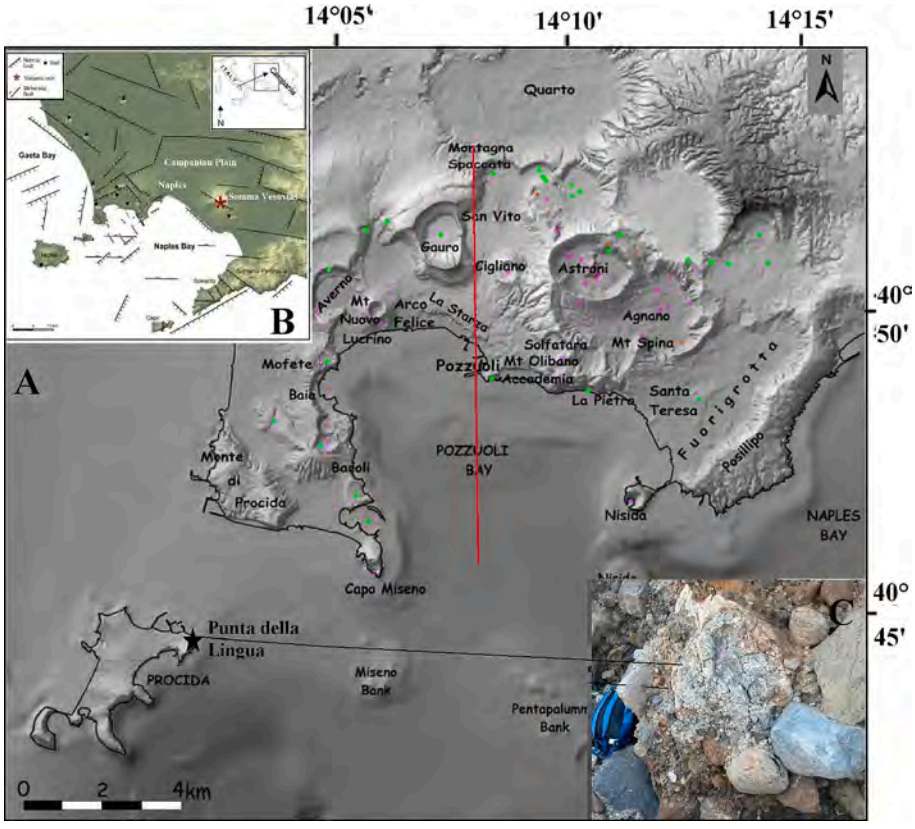

Fig. 1. A) Campi Flegrei digital map and B) location in the Campanian Plain. C) Photo of the skarn boulder and sample site location at Punta della Lingua, Procida Island.

1995; Fedele et al., 2008, 2016; Gebauer et al., 2014). The BM consists of 6 well-defined units, cropping out in limited exposures along the CF caldera rim; the entire sequence reaching up to 70 m in thickness (Fedele et al., 2008). One of the most peculiar units of the BM sequence is the so-called Breccia Unit (BU), a coarse, clast-supported, heterolithological breccia containing abundant lithic clasts of extremely varied origin (lavas, tuffs, plutonic rocks, sedimentary rocks, thermometamorphic rocks) and lesser amounts of trachytic-phonolitic juvenile clasts (pumice, scoria, and obsidian; Rosi and Sbrana, 1987; Melluso et al., 1995; Fedele et al., 2008; Gebauer et al., 2014; Gallo et al., 2024).

Volcanic activity between the CI and the NYT events was confined within the caldera and characterized by small explosive, mainly phreatomagmatic, eruptions (Pappalardo et al., 1999; Pabst et al., 2008). The post-NYT eruptions occurred in three periods between 15 and 10.6 kyr BP, 9.6 and 9.1 kyr and 5.5 and 3.5 kyr BP (Orsi, 2022). The post-NYT activity led to the formation of numerous monogenic volcanoes producing more than 70 eruptions, mostly explosives (e.g. Di Vito et al., 1999; Orsi et al., 2004; Fedele et al., 2011). The last eruptive event at CF was the 1538 CE historical eruption of Monte Nuovo, after which only fumarole emissions and bradyseismic events attest to the still active state of the magmatic system (e.g. Orsi, 2022 and references therein).

2.2. Previous fluid and melt inclusions studies on the BM lithic clasts

The abundant lithic clasts in the BU have been the subject of numerous studies on the FIs and MIs in their minerals. Danyushevsky and Lima (2001), studying MIs in clinopyroxene (cpx) of porphyritic mafic xenolith sampled in BU, found that they crystallized at T between 1160 and 1200 °C and from a magma matching the one that gave rise to the older Somma Vesuvius (SV) eruptions (>25 ka).

Fulignati et al. (2004), studying FIs and MIs in cpx and alkali feldspar crystals of syenitic and leuco-dioritic lithic clasts sampled in the BU deposits, found that the multiphase saline melt inclusions hosted in alkali-feldspar have salinities of 80–82.5 wt% NaCl eq., and trapping T between 870 and 975 °C. The same inclusions hosted in cpx have salinities between 77 and 79 wt% NaCl eq., and trapping T in the 795–840 °C range. The cpxs studied by Danyushevsky and Lima (2001) show higher trapping temperatures because they formed in deeper and less evolved magma.

Fedele et al. (2006) studied in detail a suite of alkali syenitic lithic clasts from BU Deposits. On the basis of FIs and MIs data along with the enrichment of a wide variety of accessory minerals (e.g. thorite, pyrite, chalcopyrite, galena) and incompatible elements (e.g., U, Zr, Th, and Rare Earth elements) they argued that CF resembles a mineralized system of the porphyry copper type at the initial stage (Burnham, 1979; Fournier, 1999). The authors report trapping temperatures between 950 and 1100 °C for MIs in alkali feldspar crystals and 52 ka formation ages based on zircon U—Th geochronology.

3. Materials and methods

3.1. Studied samples

Studied skarn xenoliths have been sampled in the lithic-rich Breccia Unit (BU) of the Breccia Museo (BM) deposits cropping out at Punta della Lingua, Procida island (Fig. 1C). During the excavation for the construction of a marine cliff, a new BM sequence that contained a skarn

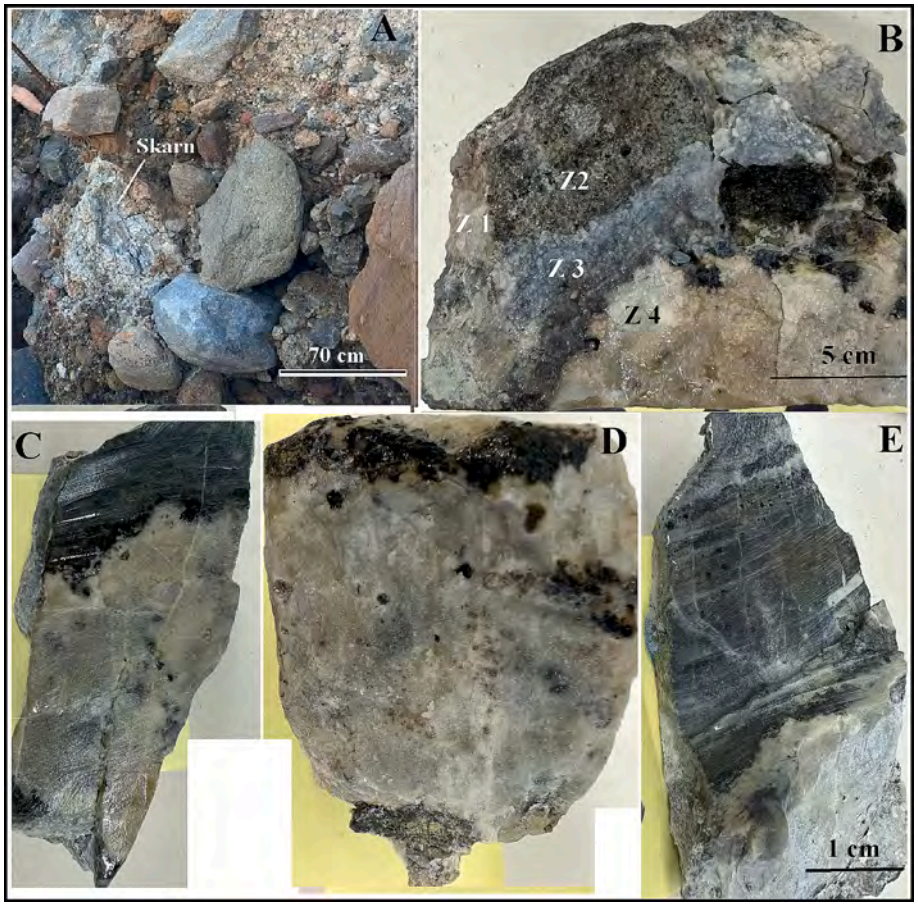

Fig. 2. A) Sampled skarn, about 70 cm large, in the lithic-rich Breccia Unit (BU) of the Breccia Museo (BM) deposits (Procida Island - Campi Flegrei). B) Sample zonation consisting of four main zones (Z1, Z2, Z3, Z4). C) Sample BM1 D) Sample BM4 E) Sample BM2. Scale bar is the same for B, C and D images.

boulder (about 70 cm in diameter) was revealed. From the latter, three samples, BM1–2-4, were taken at increasing distances from the outer surface, covering an overall length of about 16 cm (Fig. 2).

3.2. Petrographic investigations

The thin sections were carbon-coated and examined with a Hitachi SU5000 Schottky thermally assisted field emission scanning electron microscope (SEM) equipped with an Oxford Ultima 100 mm2 Energy Dispersive Spectroscopy (EDS) silicon drift detector with Oxford AZtec software. The samples were examined by SEM back-scattered electron (BSE) imaging to define points for analysis and mineral identification. We identified the mineral phases by optical petrography and by SEM peak identification and their relative intensities. For some accessory minerals where we were uncertain of their identification, we indicated that in the text. To obtain compositions for some of these mineral phases, we used the Oxford AZtec EDS beam measurement system with the extended set of factory element standardization (Supplemental Table 1). Operating conditions were 20 kV, 40 spot position (~1.7 nA probe current), 10 mm working distance, and 100 s live counting time. To check for accuracy, we noted the normalized cations to make sure they were compatible with their formulae. The Supplemental Tables (from 2 to 8) contain data for olivine, clinopyroxene, feldspar, melilite, monticellite, calzirtite, and carbonates.

3.3. FIs and MIs investigations

FI and MIs investigation in skarn-bearing minerals have been done using 300 μm thick double-polished wafer fragments. We performed 60 heating/cooling experiments of MIs hosted in olivine. For the heating experiments we employed the Linkam TS1400XY heating/cooling stage (Esposito et al., 2012) using N_2 gas flow (0.5 ± 5 % liter/min) and ca. 50 μm gold flakes as standards to calibrate the instrument at the melting point of gold (1064 °C), with heating ramps as 100 °C/min from 25 to 900 °C, 50 °C/min from 900 to 1000 °C, and 25 °C/min from 1000 to 1100 °C (Esposito et al., 2012). Based on this calibration, the error for the T during experiments is around 5 °C. Only a few MIs were brought to 1100 °C; the majority, to avoid decrepitation, was heated up to 1000 °C and cooled to room temperature at a variable rate between 30 and 20 °C/min. On cooling, the MIs have been quenched (T quench range between 760 °C and 890 °C) when instantaneous unmixing occurs and the immiscible liquids form different pockets in the MI. Most of the heating/cooling experiments have been filmed; one is available in the supplementary material (Supplementary video 1), and others upon request.

At the Dipartimento di Scienze dell'Ambiente e della Terra Università degli Studi di Milano-Bicocca using a HORIBA LabRAM HR Evolution, micro-Raman spectroscopy has been utilized (Frezzotti et al., 2012; Remigi et al., 2023). Analyses have been carried out on: 1) quenched MI, 2) selected MIs not heated and 3) FIs hosted in individual doubly-polished phenocrysts. The instrument is characterized by an air-cooled detector (1024 × 256 px Charge-Coupled Device) using a Peltier effect at −70 °C and a spectrometer system with an 800 mm focal distance. Micro-Raman analysis was obtained using a green laser source (532.06 nm) and a power of 75 mW. The micro-Raman spectra were obtained by focusing the beam into inclusions no more than 30 μm deep into the crystal host using a transmitted light microscope and a 100× objective with a numerical aperture of 0.90 (spatial resolution ≤ 1 μm^3). In addition, for the micro-Raman spectra acquisition, we used the 600 grating (grooves/mm) along with the 100 μm diameter confocal pinhole, resulting in a spectral per-pixel resolution of ~1.43. We obtained spectra with acquisition time from 30 to 60 s and two accumulations. The instrument was calibrated using a silicon carbide (SiC) standard based on the micro-Raman system Service (Hutsebaut et al., 2005). Micro-Raman analysis of the inclusions was performed at T 20 ± 0.5 °C. We used the software fityk 1.3.1 for all micro-Raman spectra to apply a baseline correction and to fit the peak with a pseudo Voigt function (e.g., Frezzotti et al., 2012).

4. Results

4.1. Petrography

Representative polished thin sections were prepared from a 16 cm section (Fig. 2) of the boulder and examined by optical and electron microbeam petrography. The samples display a large variability in rock textures and mineral assemblages. A clear zonation, consisting of four main zones, has been recognized (Fig. 4 and Supplementary Fig. 1).

Zone 1 represents the outermost part of the boulder. It is a medium to coarse-grained allotriomorphic syenite consisting of large alkali feldspar grains that range in composition from An3Ab26Or71 to An4Ab38Or59 and less abundant plagioclase, hedenbergite, and titanomagnetite. The plagioclase composition averages An42Ab51Or7, large (up to 600 μm) anhedral to subhedral hedenbergite are unzoned, interstitial, and have a composition of En13Fs39Wo48. Accessory minerals are common zirconolite, fluorbritholite-(Ce), titanite, and rare baddeleyite and probable

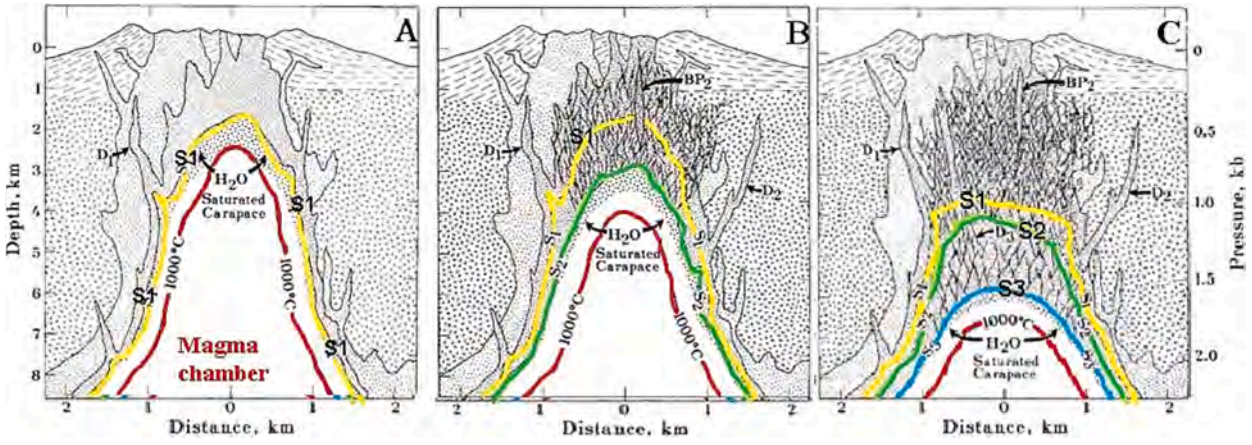

Fig. 3. Schematic cross section through a hypothetical granodiorite porphyry-copper system in development (from Burnham, 1979). A) Initially, the system is open, and any volatiles by solidification (S1) escape; an impermeable rock rind forms at the top of the magma chamber, isolating the underlying magma, and only conductive heat loss is permitted. B) The crystallization front migrates downward (S2) along with H_2O-saturated carapace. C) solidification proceeds (S3), and the magma chamber gets deeper and deeper over a long time. BP and D schematically represent a breccia pipe and dike that formed as a result of wall rock failure in the different stages (1,2,3).

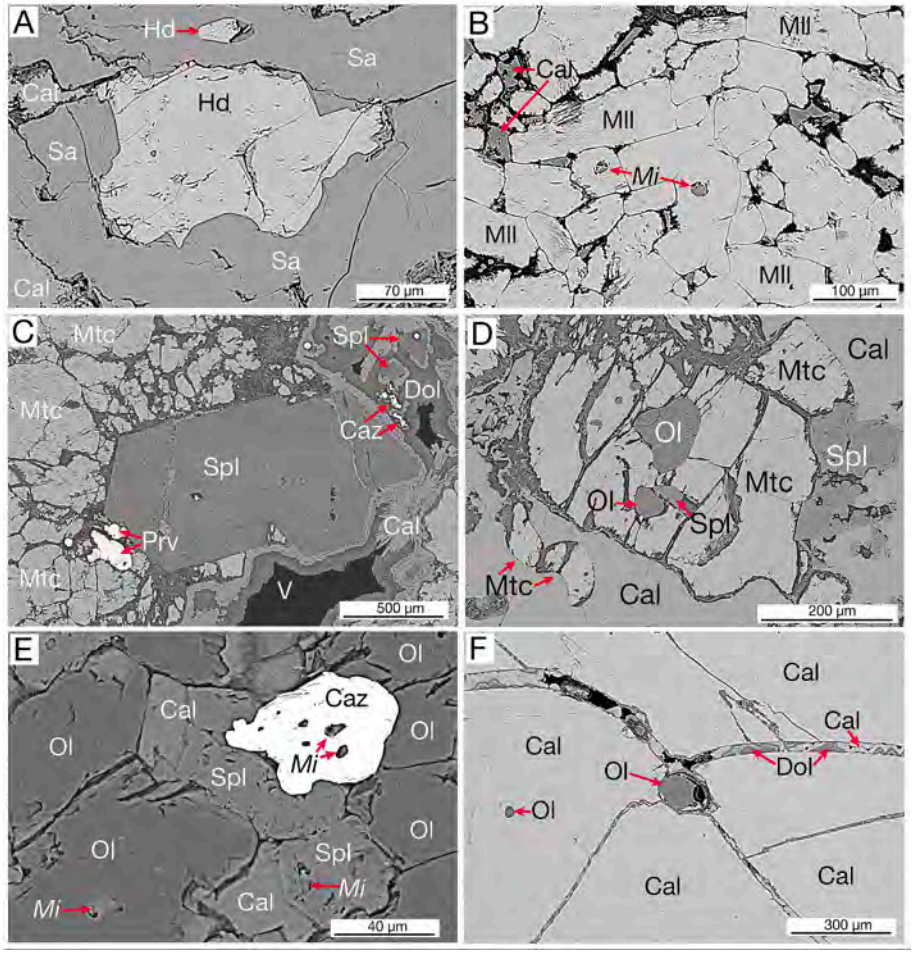

Fig. 4. Representative BSE-SEM images of the 4 zones. A) Zone 1, sanidine (Sa) with intersertal hedenbergite (Hd), and late stage calcite (Cal). B) Zone 2, melilite (Mll) crystals with two melt inclusions (Mi), and late stage calcite (Cal). C) Zone 3, spinel (Spl), monticellite (Mtc) that has been fractured and partially altered, and subhedral crystals of perovskite (Prv), and calzirtite (Caz). Late stage deposition of calcite (Cal), and dolomite (Dol) has formed voids (V). D) Zone 3, large and small crystals of monticellite (Mtc), with olivine (Ol) and spinel (Spl) inclusions. Subhedral to euhedral spinel (Spl) and late-stage calcite (Cal). E) Zone 3, olivine-rich (Ol) area with spinel (Spl), calcite (Cal), and calzirtite (Caz). Melt inclusions (Mi) in olivine, spinel and calzirtite are shown. F) Zone 4, calcite (Cal) with two olivine crystals (Ol). Late-stage fractures are filled with zoned calcite (Cal) and dolomite (Dol).

baghdadite.

Zone 2 is dominated by medium- to fine-grained melilite crystals, locally showing regular crystalloblastic textures with triple junctions (Fig. 4B). Some olivine crystals are also present ($Fo_{97–98}$). The melilite composition ranges from Gh41Åk59 to Gh62Åk38; FeO varies from 0.9 to 2.5 wt%, and Na_2O varies from 0.4 to 0.7 wt%. Melilite, mainly 200–300 µm in diameter, generally displays anomalous yellow-grey interference colors. Still, larger crystals (up to 500 µm) with inner patches showing anomalous blue interference colors were also observed. Some interstitial microcrystalline calcites, likely representing a late-stage cement, are locally present.

Zone 3 is the most heterogeneous, both in texture and mineral assemblage. The main mineral phases are monticellite, olivine, aluminous spinel, and calcite (Fig. 4C, D, E). Monticellite varies in composition from Mtc94 Kir6 to Mtc90 Kir10 and, in some areas, shows regular crystallographic texture with triple junctions. Olivine has a relatively constant composition (Fo97–98). The MgO content of calcite varies from 0.5 to 6.0 wt% and is texturally late in the assemblage in many places. Large (up to 2 mm) euhedral green spinel crystals have a FeO content of ~9 wt%, whereas smaller aluminous green spinel, usually associated with olivine, are slightly more hercynitic (FeO ~14 wt%). Common accessory minerals are perovskite, calzirtite (Fig. 4C, D, E), fluorite, and anhydrite; less common are probable kimzeyite garnet and rare periclase. Perovskite occurs as anhedral to euhedral crystals, with the large (~125 µm) anhedral masses zoned in REEs, Nb and Th, whereas smaller (30 µm) perovskite tends to be euhedral and unzoned. Calzirtite is unzoned and stoichiometric.

Zone 4 (Fig. 4F) is a nearly monomineralic, medium- to coarse-grained granofelsic calcite (MgO ~0.4 wt%) marble with minor accessory olivine (Fo97–98). All 4 zones have been affected by late-stage fracturing with vein filling and some alteration. The common vein and alteration components are calcite, dolomite, chlorite, and a serpentine phase.

4.2. FIs and MIs results

This paper focuses on two types of inclusions, CO_2-rich FIs and MIs, because they are the only ones present in the crystals. The former are uncommon.

4.2.1. CO_2-rich fluid inclusions

CO_2-bearing fluid inclusions are uncommon in the unheated olivine, sanidine and calcite hosts investigated. They have been found mainly in zone 1 in sanidine. In other zones and hosts, FIs are rare; when observed, they are <2 µm. They show spherical to subspherical shapes with a vapor phase only and are <5 µm. Most measures 3 µm (Fig. 5A) and they are along fracture planes (secondary FI), about 30 are randomly isolated inside the crystal hosts (primary FI). Isolated FIs analyzed by micro-

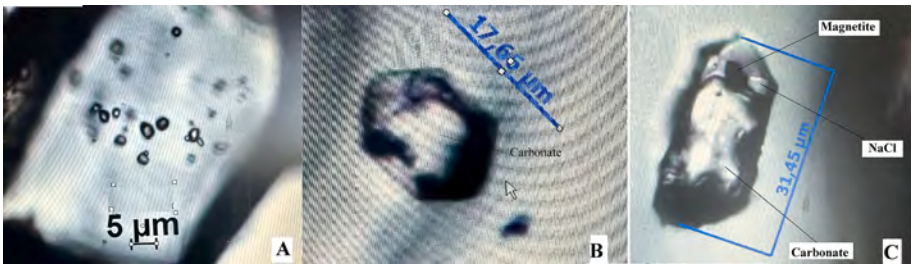

Fig. 5. FIs and MIs pictures at room temperature: A) CO_2 FIs in sanidine; B) and C) MIs named Saline Carbonate Melt Inclusions (SCMI) in olivine.

Raman spectroscopy are empty except for 10 FIs that show CO_2 signals. Of these 10 CO_2-rich FI, three show H_2S signals along with CO_2 (Table 1). The CO_2 signals of these Fis are characterized by the Fermi diad peaks. For one FI, the Fermi diad peaks were weakly above the background and could not be considered for the density calculation (Remigi et al., 2021; Bodnar and Frezzotti, 2020). Three of the FIs are strongly asymmetric, but the other FIs show CO_2 Fermi diad peaks, which do not show this asymmetry. For FIs that do not show either asymmetric CO2 peaks or H2S signals, we calculated the density based on the Remigi et al. (2021) densimeter. The density calculated ranges from 0.11 to 0.14 g/cm^3 (Table 1). These densities likely have at least >20 % 1σ error based on the uncertainty of peak positions as reported by Remigi et al. (2021), and they need to be taken with caution. Also, a possible optically undetectable film (<1 μm) of liquid CO_2 could be present at the T of measurements (20 °C). Thus, the estimated densities can be used only to calculate the minimum P of entrapment based on an EOS (Pitzer and Sterner, 1994) and assume a range of T from 900 to 1100 °C. Pressures calculated using this method range from 26 to 44 MPa, corresponding to depths from 1 to 2 km (Table 1). The H_2S signals of the three FIs are relatively weak and show an asymmetric shape, indicating that it is present as a gas phase, likely corresponding to relatively low density (e.g., Salmoun et al., 1994).

4.2.2. Melt inclusions

The MIs suitable for experiments have been found primarily on olivine and spinel in zones 2 and 3. They have very variable dimensions, from a few microns to >60 μm, most measures 15 μm andshows a polygonal shape at room temperature (RT), showing numerous daughter crystals and the shrinkage bubble(s) (Fig. 5B and C). Fig. 6 shows SEM-BSE images of representative MIs in Zone 3 in olivine and spinel. Commonly, calcite, along with anhydrite, fluorite, monticellite, baryte, uraninite, chlorapatite, pyrrhotite, galena and scheelite have been detected in these MI.

Selected MIs have been investigated by microthermometry and show roughly the same behavior during heating and cooling experiments. Upon heating (rate 20 °C/min) at about 160 °C, droplets of hydrosaline liquid start to move and converge in a pocket that gradually expands. The NaCl daughter crystals (identified with good approximation by optical microscopy) melt completely at T between 620 and 670 °C. Several pockets containing immiscible liquids form in a range of T between 730 and 750 °C (Fig. 7A), they progressively shrink with increasing T (Fig. 7B) and homogenize at 920 °C (Fig. 7C). On further heating, MIs completely homogenize (i.e., shrinkage bubble disappearance) between 980 and 1060 °C. To avoid decrepitation for quenching, MIs was not always wholly homogenized and cooling experiments started at about 1000 °C. After MIs homogenization or when it is almost homogenized, the cooling experiment starts (rate 20 °C/min). The shrinkage bubble forms between 880 and 1000 °C; cooling on, between 790 and 750 °C, an instantaneous unmixing occurs (Fig. 7D) (see also the Supplementary video 1 showing clips of instant unmixing for different MI) and then pockets of immiscible liquid form (Fig. 7E and F). Since pockets of immiscible liquids form in the same way, both by heating and cooling, the process is reversible.

At T between 520 and 450 °C, NaCl crystallizes from a moving hydrosaline liquid in the MI; the latter's droplets are visible up to 150 °C. Note that even during heating experiments, the droplets of hydrosaline liquid begin to form at about 160 °C.

Micro-Raman spectrometry analyses have been performed on the previously quenched (between 760 and 890 °C) to determine the qualitative geochemical composition of the observed immiscible liquids in MI. Unheated MIs have also been analyzed to compare the geochemical compositions (Fig. 8A and B, Table 2). Fig. 8C and D show MIs after quenching and compositions by micro-Raman spectrometry analyses. After that, unmixing occurs in MI, carbonate liquid, silicate melt (glass) and hydrosaline liquid (brine) form the observed separate pockets (Fig. 7A). Hydrosaline liquid (brine) has been detected based on heating/cooling experiments. The analyzed MIs have been named saline-carbonate melt inclusions (SCMI) to reflect their composition.

All the heated and unheated SCMI analyzed are hosted in olivine and show carbonate micro-Raman signals. The most frequent carbonate detected is Mg-calcite in unheated or heated SCMI (Supplementary Fig. 2, Table 2). Many of the SCMI include a strong peak in the range of 1001–1019 cm^{-1}, often accompanied by a peak at 469–477 cm^{-1}. These signals are characteristics of sulfate vibrations (e.g., 1018 cm^{-1} anhydrite). In one case, all peaks of cesanite [$Na_3Ca_2(OH)(SO_4)_3$] were identified (Frezzotti et al., 2012; Supplementary Fig. 3), along with gypsum. For gypsum, however, the higher wavelength numbers could not be investigated for the high fluorescence of the samples. Additional

Table 1
Calculated density based on the Remigi et al. (2021) densimeter for FIs that do not show neither asymmetric CO_2 peaks nor H_2S signal.

ID	Host	V-	V+	Delta V	Density	Notes	Pressure (Mpa)*	Depth (km)**
BM1 cip2-FI-P5	Sanidine	1286.42	1389.38	102.96		V- asymmetrical		
BM1 cip2-FI-P6	Sanidine	1286.48	1389.48	103.00	0,11		26–31	0.96–1.14
BM1 cip2-FI-P7	Sanidine	1286.82	1389.58	102.76		V- asymmetrical		
BM1 cip2-FI-P8	Sanidine	1286.29	1389.33	103.04	0,14		33–44	1.22–1.63
BM1 cip2-FI-P9	Sanidine	1286.80	1389.80	103.00		H_2S present		
BM1 cip2-FI-P11	Sanidine	1286.46	1389.47	103.01	0,12		28–34	1.04–1.26
BM1 cip2-FI-P12	Sanidine	1286.42	1389.35	102.93		V- asymmetrical		
BM1 cip2-FI-P13	Sanidine	1286.63	1389.62	102.99		H_2S present		
BM1 cip2-FI-P14	Sanidine	1286.65	1389.67	103.02		H_2S present		

* EOS (Sterner and Pitzer, 1994).
** 27 Mpa/km.

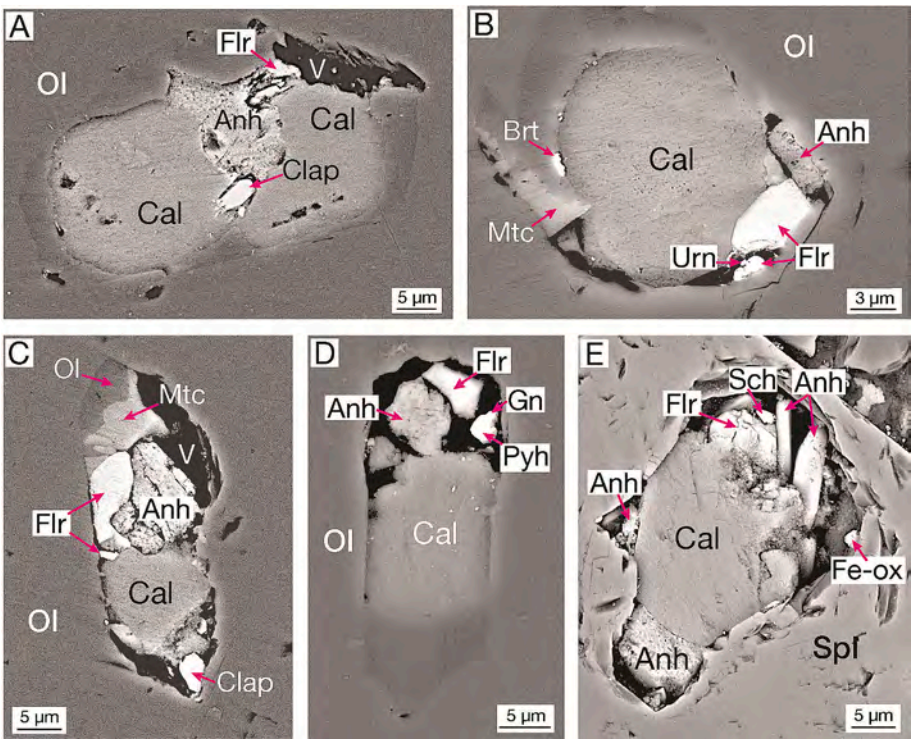

Fig. 6. Representative SEM BSE images showing inclusions in olivine (Ol, Fo97) and spinel (Spl, 14 wt% FeO) crystals from Zone 3 of the investigated BM skarn samples. A: 60 µm inclusion containing calcite (Cal, 1.5 wt% MgO), anhydrite (Anh), fluorite (Flr), chlorapatite (Clap, V-, As-bearing), and a void (V). B: 20 µm inclusion containing Cal (1.4 wt% MgO), Anh, Flr, monticellite (Mtc), baryte (Brt, 1 wt% SrO), and uraninite (Urn). C: 50 µm inclusion containing Cal (2 wt% MgO), Anh, Flr, Mtc, Clap (V-bearing), and a V. In many of the inclusions, Ol was precipitated on their walls. D: 30 µm inclusion containing Cal (1.4 wt% MgO), Anh, Flr, pyrrhotite (Pyh) and galena (Gn). E: 40 µm inclusion containing Cal (1.2 wt% MgO), Anh, Flr, iron oxide (Fe-ox), and scheelite (Sch, Mo-bearing).

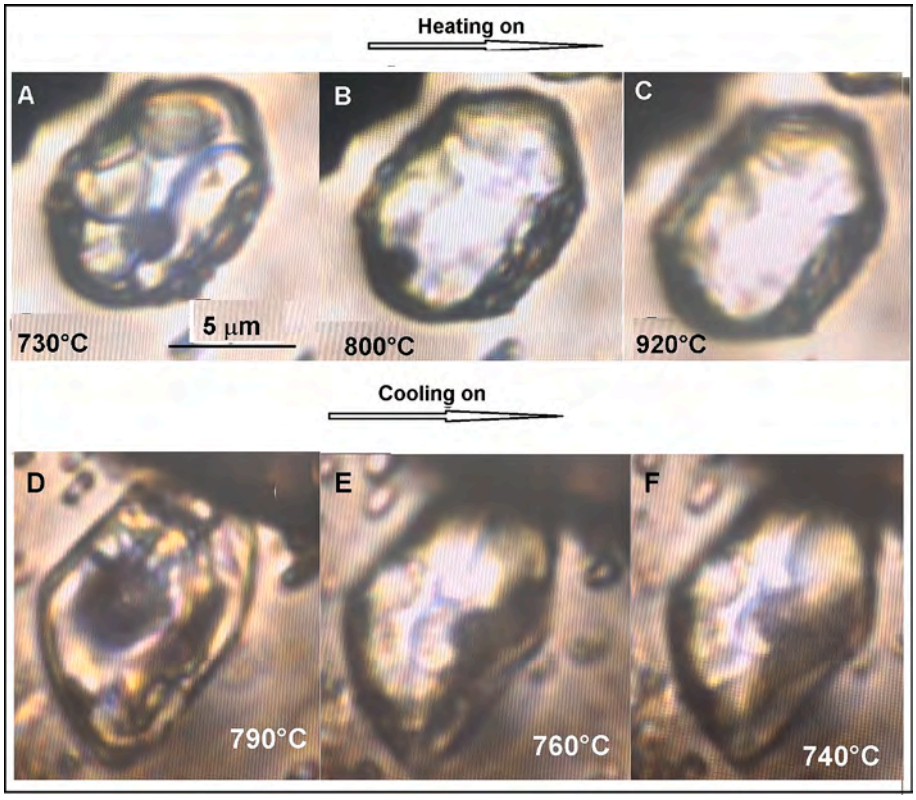

Fig. 7. Pictures of Saline Carbonate Melt Inclusions (SCMI) during heating/cooling experiments. On heating: A) the homogenized melt at 730 °C form separate pockets of immiscible liquids; B) the pockets shrink C) at 920 °C the pockets containing immiscible liquids homogenize. On cooling: D) instant unmixing occurs, E) different pockets of immiscible liquids form and F) on cooling, they grow up.

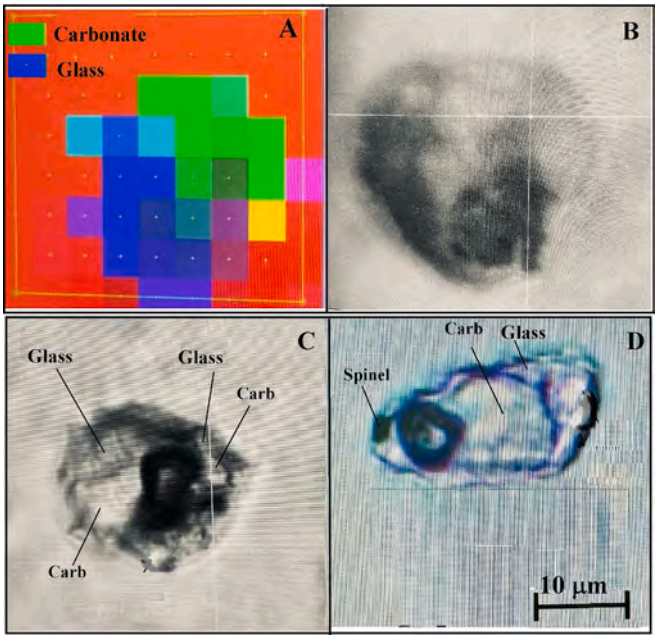

Fig. 8. A) A rectangle map of 72 points of micro-Raman spectroscopy analyses of the unheated Saline Carbonate Melt Inclusions (SCMI) showed in B. C and D) Different SCMI were quenched and analyzed by micro-Raman spectroscopy. The scale refers to all SCMI.

phases recognized in SCMI are spinel, anatase, and glass. Importantly, CO_2 was not detected in any SCMI shrinkage bubbles.

5. Discussion

5.1. Petrology of BM skarn xenoliths

According to the International Union of Geological Sciences (IUGS), skarn is a term denoting metasomatic rocks that form at the contact between a silicate rock (or melt) and a carbonate rock (Fettes and Desmons, 2007). All skarn types are generally characterized by complex alternations of different levels with varying mineral assemblages and/or textures, giving rise to a closely spaced zonation at the cm- to the mm-scale [see Meinert, 1998; Meinert et al., 2005; Knuever et al., 2023a for a review]. Controlling factors of zonation can include depth of formation, magma composition, timing of the exsolution of magmatic aqueous fluids, redox state of the magma and redox state of the wall rocks. Regarding magma composition, volatiles can also affect the formation of skarns and zoning patterns.

The four distinctive mineral zones identified in the samples studied testify to the complex magma-carbonate interaction processes. Zone 1 reasonably represents the crystallization front of the magma which gave rise to the formation of syenite rocks. This passes to the well-equilibrated, melilite-dominated Zone 2. The presence of melilite, known to be stable at generally high T (e.g. ~ 900 °C or > 950 °C at 100 MPa; Tracy and Frost, 1991; Whitley et al., 2020), is consistent with the temperature measured by SCMI. Zone 3 is highly heterogeneous in texture and mineral assemblage, rich in accessory minerals containing elements commonly transported by hydrothermal fluids. Olivine-bearing SCMI crystallized in this zone and trapped melts during its growth. Zone 4 is nearly monomineralic and represents the thermometamorphic transformation of the carbonate country rock. For the purposes of this paper, the detailed composition of the accessory minerals by electron microprobe is not relevant, but in a future project the complex suite of accessory minerals will be studied in detail, with particular attention to zirconium minerals.

The abundance of Mg-bearing skarn minerals (olivine, clinopyroxene, melilite), coupled with the absence of wollastonite, suggests that at CF, the carbonate country-rock is not pure limestone (as in the case of the Merapi skarn samples; Whitley et al., 2020). A mixed limestone-dolostone country rock was also proposed for the skarn xenoliths found in the pyroclastic products of the Somma-Vesuvius eruptions (79 CE, Pollena 472 CE, 1631 CE and 1944 CE; Fulignati et al., 2000, 2001, 2004; Pascal et al., 2011; Jolis et al., 2015; Lima and Esposito, 2024). The latter are characterized by mineral assemblages that generally feature variable Ca-Al-rich "fassaitic" clinopyroxene abundances. The Colli Albani skarn samples (Gaeta et al., 2009; Di Rocco et al., 2012) also have abundant Ca-Al-rich ("Ca-Tschermak-rich") clinopyroxene, which have higher MgO and lower Al_2O_3 and FeO with respect to Somma-Vesuvius counterparts. Such compositional differences likely reflect the least evolved, more silica-undersaturated nature of the Colli Albani magmas and the fact that the Colli Albani basement is known to consist of dolostone country rock (e.g. Di Rocco et al., 2012). The notable absence of Ca-Al-rich clinopyroxene in CF skarn samples could be explained by fluorine (fluorbritholite is a common accessory mineral) that can dramatically increase the solubility of Al in hydrothermal fluids by forming strong Al—F complexes (Tagirov et al., 2002).

Table 2
Heated and unheated Saline Carbonate Melt Inclusions (SCMI) analyzed by micro-Raman spectroscopy.

ID	Type	Host	Found in SCMI				
			Carbonate	Spinel	Glass***	CO_2	H_2S
BM4 cip 22-MI1	SCMI	olivine	yes	yes	yes	no	no
BM4 cip 9-MI1	SCMI	olivine	yes	yes	yes	no	no
BM4 cip 9-MI2	SCMI	olivine	yes	no	no	no	no
BM4 cip30-MI1	SCMI	olivine	yes	yes	yes	no	no
BM4 cip30-MI2	SCMI	olivine	yes	yes	yes	no	no
BM4 cip33-MI1	SCMI	olivine	yes**	no	yes	no	no
BM4 cip21-MI1	SCMI	olivine	yes	probable	probable	no	no
BM4 cip 16-MI1	SCMI	olivine	yes**	yes	yes	no	no
BM4 cip 13-MI1	SCMI	olivine	yes	yes	yes	no	no
BM4 cip 13-MI2	SCMI	olivine	yes	yes	yes	no	no
BM4 cip 34-MI1	SCMI*	olivine	yes	yes	yes	no	no
BM4 cip 34-MI2	SCMI*	olivine	yes	yes	yes	no	no
BM4 cip 34-MI3	SCMI*	olivine	yes	yes	yes	no	no
BM4 cip 35-MI1	SCMI	olivine	yes	no	yes	no	no
BM4 cip 35-MI2	SCMI	olivine	yes	no	yes	no	no

* Not heated.
** Possible presence of strontianite.
*** Possible presence of sulphate.

5.2. Campanian Ignimbrite shallow magma chamber depth

The pressures calculated for the shallow CI magma chamber by CO_2 FIs hosted in sanidine range from 26 to 44 MPa, corresponding to depths of about 1 to 2 km (Table 2). As discussed above, the latter can only be used to calculate the minimum P. This shallow depth would approach the depth ranging from 2 to 4 km indicated by several studies (e.g. Milia and Torrente, 1999; Milia et al., 2003). On the other hand, if CF represents a porphyry copper system at the embryonic stage, as discussed in the introduction, as shown in Fig. 3 magma chamber and the crystallization front (S1-S2-S3 in Fig. 3A, B and C) deepens over time along with the H_2O-saturated carapace. Based on data by MIs in previous studies (Danyushevsky and Lima, 2001), it is possible to hypothesize that the deep CF magmatic system (likely feeding CI, at T between 1160 and 1200 °C) was geochemically similar to the one feeding the old SV eruptions >25 kyr. Instead, from the ages of 52 ka, obtained by zircon U—Th geochronology for CI (Fedele et al. (2006), it could be possible to argue that CI magma had a long repose time. The latter has been calculated by Gebauer et al. (2014) of 9.1 kyr.

5.3. Campanian Ignimbrite magma composition at the top of the magma chamber

Melt inclusions (MI) are microscopic droplets of magma trapped in growing crystal microcavities; they are closed microsystems that preserve valuable information on pre-eruptive magma composition, including the volatile content that escapes during the eruptions. On heating, MIs homogenize, and the homogenization temperatures (Th) indicate the host crystallization temperature if the confining pressure of the system is relatively low (Roedder, 1979; Cannatelli et al., 2016 and references therein; Esposito, 2021, Rose-Koga et al., 2021; Wallace et al., 2021). The SCMI are assumed to reproduce, on a small scale, the behavior at larger scale of the melt that forms in the transition zone between the magma dominated system and hydrothermal dominated system. This means that the melt was homogeneous at T between 980 and 1060 °C, during olivine crystallization, and instantaneous unmixed between 790 and 750 °C leading to the formation of three immiscible liquids: carbonate, silicate (glass) and hydrosaline (Fig. 7D, E, F, Supplementary video 1). Instantaneous unmixing has already been reported in SV skarn MIs (Fulignati et al., 2001; Gilg et al., 2001; Lima and Esposito, 2024) studied for different purposes.

In the transition zone, many chemical reactions can occur, like high-temperature hydrolysis with phase separation and formation of other phases (Veksler, 2004; Veksler and Charlier, 2015). Carbonate country rocks melting increase CO_2, Ca, and Mg concentrations (Lentz, 1999, 2017). In SCMI, high Ca and Mg content have been found by micro-Raman analysis, and contrary to our initial predictions, we did not detect any trace of CO_2 in their shrinkage bubble as a free gas species, based both on microthermometric investigations and on micro-Raman spectroscopy.

As previously discussed, trapped melt is enriched also in a wide variety of trace elements (e.g. Zr, F, Nb, Th, and Rare Earth Elements) generally transported by magmatic fluids and found in porphyry copper systems (Fig. 3). Fedele et al. (2006) reached the same conclusion studying the alkali syenitic samples from the same BU deposit at CF. In addition, the ore minerals present in the cores of the Mofete and San Vito wells in the CF area, and attributable to a porphyry mineralized system, have recently been studied in detail (Belkin and De Vivo, 2023; Belkin et al., 2024).

Until now immiscibility, between carbonate, silicate and hydrosaline liquids has been widely documented at SV, as already mentioned, and in other subvolcanic Italian systems as well, such as the islands of Ponza (Belkin et al., 1996; De Vivo et al., 2006), Ventotene (De Vivo et al., 1995; Fulignati et al., 2005), and Pantelleria, the latter in the Sicily Channel (De Vivo et al., 1992, 1993, 2006; Lowenstern, 1993, 1994).

5.4. Inferences from unmixing behavior

The above discussion raises two main issues: 1) Although carbonate melting should increase Ca, Mg and CO2 in the melt that form in the transition zone, CO_2 was not found in the SCMI bubbles. How can this be explained? 2) Why does the instantaneous unmixing happen? It could be essential to answer these questions to understand the role of carbonate reacting with magma.

We interpret the lack of CO_2 as a free gas species in the trapped melt due to a series of reactions. When carbonates melt in the transition zone, where H_2O by magmatic system second boiling accumulate, at the top of the magma chamber, $CaCO_3$ dissolution produces $CaO + CO_2$ at high $T > 980$ °C, then CaO and CO_2 react with H_2O forming $Ca(OH)_2$ and H_2CO_3 respectively, we assume that both dissolved into homogeneous melt. Upon cooling unmixing occurs and $Ca(OH)_2$ and H_2CO_3 form again **$CaCO_3$** and water as a by-product, at $T < 790$ °C, according to the following equations:

$$\mathbf{CaCO_3} = CaO + CO_2 \; T > 980^{\circ}C \quad (1)$$

$$CaO + H_2O = Ca(OH)_2 \; T > 980^{\circ}C \quad (2)$$

$$CO_2 + H_2O = H_2CO_3 \qquad T > 980^{\circ}C \quad (3)$$

$$Ca(OH)_2 + H_2CO_3 = \mathbf{CaCO_3} + 2H_2O \; T < 790^{\circ}C \quad (4)$$

The first three reactions occur at high temperatures (>980 °C), typical of the boundary of the magma chamber with the country rock (e.g. carbonate), and the last Reaction (4) at a later time along with unmixing, at a lower temperature (e.g. between 750 and 790 °C) as evidenced by SCMI heating/cooling experiments reported in previous paragraphs. When at lower temperature, unmixing occurs (see Supplementary video 1), two moles of H_2O are instantly released, allowing in SCMI the formation of the immiscible hydrosaline liquid as H_2O dissolves salts (e.g. NaCl). As previously discussed, in the SCMI at $T <$ 750 °C, there are three immiscible liquids: carbonate, silicate (glass) and hydrosaline. Reactions (1)–(3) represent an efficient mechanism for retaining H_2O with the absorption of two moles of H_2O per each carbonate mole; Reaction (4) represents an efficient mechanism for releasing H_2O instantly. Reactions (1)–(3) can only occur in the presence of abundant H_2O as in the area of the saturated carapace (Fig. 3). Since SCMI is homogeneous at the entrapping temperature, we can infer that $Ca(OH)_2$ and H_2CO_3 are dissolved in the melt that form by carbonate interactions. This is the most relevant assumption we adopt in the present paper for its implication during melt rise, as described in the next paragraph. The observed instantaneous unmixing on cooling would be due to the release of water produced by Reaction (4). The latter leads to a new vision of the processes that can affect eruptions explosivity. If, for instance, the melt (modified magma) residing at the top of the shallow magma chamber gets involved in an eruption, on cooling at T < 790 °C it unmixes releasing water that at these temperatures exist as highly superheated vapor or gas with a very high energy content.

These reactions, although studied on a micrometric scale, have been considered a simulation of what happens on a large scale in the brittle-plastic transition zone that forms between the magmatic-dominant system and the hydrothermal-dominant system. Therefore, it is not the size of the system that is relevant, but its behavior. The amount of water released by Reaction (4) depends on the amount of melt that forms in the transition zone that could open the eruption.

5.4.1. New vision on magma intrusions and its consequence on the opening phase of the eruptions

Here we hypothesize possible consequences on the propagation of dykes, associated with the occurrence of the above chemical Reaction (4). The occurrence of Reaction (4), at lower temperatures, may play a crucial role in the propagation of dykes during a volcanic unrest

associated with magma intrusion. In fact, once the rocks at the top of the magma chamber are fractured and magma begins to intrude, we can reasonably assume that the melt formed by carbonate interaction, near the top of the magma chamber is the first that intrudes into the fractures and, as seen previously, contains a much higher quantity of dissolved water with respect to the same uncontaminated magma which did not experience the contact with the carbonate. As the dyke propagates upwards in the colder rocks it cools significantly increasing its viscosity, until it may not be able to propagate in the narrow fractures, and halts. Instead, when the temperature reaches the unmixing temperature, a new quantity of entrapped water becomes immediately available with the consequence of pressurizing the tip of the dike, facilitating the opening of the fracture, and allowing it to propagate up to the surface. We can further hypothesize that under this condition, the opening phase of the eruption can be a phreatic explosion caused by the vaporization of the H_2O at the top of the dyke.

6. Conclusions

Recently it has been proposed (e.g. Knuever et al., 2022, 2023b; Colucci et al., 2024) that magma– carbonate country rock interaction can occur on different timescales, that range respectively from several thousand of years to hours or even shorter, and that short-term magma-carbonate interaction could represent a plausible mechanism to trigger eruptions and enhance the explosivity (Deegan et al., 2010; Sottili et al., 2010; Freda et al., 2011; Troll et al., 2012; Jolis et al., 2015; Blythe et al., 2015; Knuever et al., 2023b).

In this study, it has been demonstrated, through heating/cooling experiments on saline carbonate melt inclusions (SCMI), that the interaction between the magma and the carbonate country rock, in the transition zone between a magma dominated system and hydrothermal dominated system, allows the formation of a melt (modified magma). The latter is homogeneous at $T > 980$ °C. Upon cooling at $T < 790$ °C, it instantly unmixes, giving rise to the formation of three immiscible liquids, a silicate (glass), a carbonate and a hydrosaline (brine). Considering that the modified magma resides at the top of the shallow magma chamber, a new vision on mechanisms for the propagation of dykes and for enhancing the ongoing eruptions explosivity is proposed. The formation of the carbonate immiscible liquid ($CaCO_3$) at lower temperatures instantly plays a fundamental role as $Ca(OH)_2$ from the melt takes one mole of CO_2 to produce $CaCO_3$ and releases instantly two moles of H_2O immediately available with the consequence of pressurizing the tip of the dyke, facilitating the opening of the fracture and allowing the dyke to propagate up to the surface. In addition, during an ongoing eruption, instantaneous unmixing and the provision of water can trigger its explosivity.

From this perspective, interesting issues emerge from the results of this study. First of all, the detailed thermochemistry of the above-mentioned Reactions (1)–(4). What chemical-physical parameters can control the unmixing, the role of magma compositions, and its residence time in the shallow chamber.

Supplementary data to this article can be found online at https://doi.org/10.1016/j.jvolgeores.2025.108405.

CRediT authorship contribution statement

Annamaria Lima: Writing – review & editing, Writing – original draft, Visualization, Validation, Supervision, Methodology, Investigation, Formal analysis, Data curation, Conceptualization. **Giovanni Macedonio:** Writing – review & editing, Writing – original draft, Validation, Supervision, Methodology, Funding acquisition, Formal analysis, Conceptualization. **Rosario Esposito:** Writing – review & editing, Writing – original draft, Validation, Supervision, Methodology, Investigation, Formal analysis, Data curation, Conceptualization. **Harvey E. Belkin:** Writing – review & editing, Writing – original draft, Validation, Supervision, Methodology, Investigation, Formal analysis, Conceptualization.

Declaration of competing interest

The authors declare that they have no known competing financial interests or personal relationships that could have appeared to influence the work reported in this paper.

Acknowledgments

We thank Frank Spera and Maria Luce Frezzotti for their review and suggestions, Lorenzo Fedele for his valuable suggestions and comments of the first drafts. PRIN2022 “CRUStal CArbon: exploring the role of the crust in the C cycle (CRUSCA)” (project n°2022HA8XCS) is acknowledged by R. Esposito.

Data availability

Data will be made available on request.

References

Anikovich, M.V., Sinitsyn, A.A., Hoffecker, J.F., Holliday, V.T., Popov, V.V., Lisitsyn, S. N., Forman, S.L., Levkovskaya, G.M., Pospelova, G.A., Kuz'mina, I.E., Burova, N.D., Goldberg, P., Macphail, R.I., Giaccio, B., Praslov, N.D., 2007. Early Upper Paleolithic in eastern Europe and implications for the dispersal of modern humans. Science 315, 223–226. https://doi.org/10.1126/science.1133376.

Belkin, H.E., De Vivo, B., 2023. Compositional variation and zoning of epidote supergroup minerals in the Campi Flegrei geothermal field, Naples, Italy. Eur. J. Mineral. 35, 25–44. https://doi.org/10.5194/ejm-35-25-2023.

Belkin, H.E., De Vivo, B., Lima, A., Török, K., 1996. Magmatic silicate/saline/sulfur-rich/CO_2 immiscibility and zirconium and rare-earth element enrichment from alkaline magma chamber margins: evidence from Ponza island, Pontine Archipelago, Italy. Eur. J. Mineral. 8 (5), 1401–1420.

Belkin, H.E., McAleer, R.J., De Vivo, B., 2024. Ore mineralization in the Mofete and San Vito geothermal fields, Campi Flegrei volcanic complex, Naples, Italy. J. Geochem. Explor. 264, 107556. https://doi.org/10.1016/j.gexplo.2024.107556.

Blythe, L.S., Deegan, F.M., Freda, C., Jolis, E.M., Masotta, M., Misiti, V., Taddeucci, J., Troll, V.R., 2015. CO2 bubble generation and migration during magma–carbonate interaction. Contrib. Mineral. Petrol. 169, 1–16. https://doi.org/10.1007/s00410-015-1137-4.

Bodnar, R.J., Frezzotti, M.L., 2020. Microscale chemistry: Raman analysis of fluid and melt inclusions. Elements 16 (2), 93–98.

Bodnar, R.J., Cannatelli, C., De Vivo, B., Lima, A., Belkin, H.E., Milia, A., 2007. Quantitative model for magma degassing and ground deformation (bradyseism) at Campi Flegrei, Italy: implications for future eruptions. Geology 35 (9), 791–794. https://doi.org/10.1130/G23653A.

Burnham, C.W., 1979. Magmas and hydrothermal fluids. In: Barnes, H.L. (Ed.), Geochemistry of Hydrothermal Ore Deposits. Wiley, New York, pp. 71–136.

Cannatelli, C., Doherty, A.L., Esposito, R., Lima, A., De Vivo, B., 2016. Understanding a volcano through a droplet: a melt inclusion approach. J. Geochem. Explor. 171, 4–19. https://doi.org/10.1016/j.gexplo.2015.10.003. Special Issue; Ni et al., Eds.

Colucci, S., Brogi, F., Sottili, G., Montagna, C.P., Papale, P., 2024. Short-term magma-carbonate interaction: a modelling perspective. Earth Planet. Sci. Lett. 628 (2024), 118592. https://doi.org/10.1016/j.epsl.2024.118592.

Danyushevsky, L.V., Lima, A., 2001. Relationships between Campi Flegrei and Mt. Somma volcanism: evidence from melt inclusions in clinopyroxene phenocrysts from volcanic breccia xenoliths. Mineral. Petrol. 73, 107–119.

De Vivo, B., Frezzotti, M.L., Mahood, G., 1992. Fluid inclusions in xenoliths yield evidence for fluid evolution in peralkaline granitic bodies at Pantelleria (Italy). J. Volcanol. Geotherm. Res. 52, 295–301.

De Vivo, B., Frezzotti, M.L., Lima, A., 1993. Immiscibility in magmatic differentiation and fluid evolution in granitoid xenoliths at Pantelleria: fluid inclusions evidence. Acta Vulcanol. 3, 195–202.

De Vivo, B., Torok, K., Ayuso, R.A., Lima, A., Lirer, L., 1995. Fluid inclusion evidence for magmatic silicate/saline immiscibility and isotope geochemistry of alkaline xenoliths from Ventotene island (Italy). Geochim. Cosmochim. Acta 59 (14), 2941–2953.

De Vivo, B., Rolandi, G., Gans, P.B., Calvert, A., Bohrson, W.A., Spera, F.J., Belkin, H.E., 2001. New constraints on the eruptive history of the Campanian volcanic plain (Italy). Mineral. Petrol. 73, 47–65.

De Vivo, B., Lima, A., Kamenetsky, V.S., Danyushevsky, L.V., 2006. Fluid and melt inclusions in the sub-volcanic environments from volcanic systems: examples from the Neapolitan area and Pontine Islands, Italy. In: Webster, J.D. (Ed.), Melt Inclusions in Plutonic Rocks, Short Course Series, 36. Mineralogical Association of Canada, Montreal, Quebec, Canada. ISBN 0-921294-36-0.

De Vivo, B., Petrosino, P., Lima, A., Rolandi, G., Belkin, H.E., 2010. Research progress in volcanology in Neapolitan area, southern Italy: a review and alternative views. Mineral. Petrol. 99, 1–28. https://doi.org/10.1007/s00710.009.0098.6.

Deegan, F.M., Troll, V.R., Freda, C., Misiti, V., Chadwick, J.P., McLeod, C.L., Davidson, J. P., 2010. Magma-carbonate interaction processes and associated CO_2 release at Merapi Volcano, Indonesia: insights from experimental petrology. J. Petrol. 51, 1027–1051. https://doi.org/10.1093/petrology/egq010.

Deino, A.L., Orsi, G., De Vita, S., Piochi, M., 2004. The age of the Neapolitan Yellow Tuff caldera-forming eruption (Campi Flegrei caldera-Italy) assessed by 39Ar/40Ar dating method. J. Volcanol. Geotherm. Res. 133, 157–170.

Di Rocco, T., Freda, C., Gaeta, M., Mollo, S., Dallai, L., 2012. Magma chambers emplaced in carbonate substrate: petrogenesis of skarn and cumulate rocks and implications for CO_2 degassing in volcanic areas. J. Petrol. 53, 2307–2332. https://doi.org/10.1093/petrology/egs051.

Di Vito, M., Isaia, R., Orsi, G., Southon, J.D., De Vita, S., D'Antonio, M., Pappalardo, L., Piochi, M., 1999. Volcanism and deformation since 12,000 years at the Campi Flegrei caldera (Italy). J. Volcanol. Geotherm. Res. 91, 221–246.

Esposito, R., 2020. Magmatism of the Phlegrean Volcanic Fields as revealed by melt inclusions. In: Vesuvius, Campi Flegrei, and Campanian Volcanism. Elsevier, pp. 141–174.

Esposito, R., 2021. Chapter 7. A protocol and review of methods to select, analyze and interpret melt inclusions to determine pre-eruptive volatile contents of magmas. In: Lecumberri-Sanchez, P., Steele-MacInnis, M., Kontak, D. (Eds.), Fluid and Melt Inclusions: Applications to Geologic Processes. Ontario, Mineralogical Association of Canada, London, pp. 163–194.

Esposito, R., Klebesz, R., Bartoli, O., Klyukin, Y.I., Moncada, D., Doherty, A.L., Bodnar, R. J., 2012. Application of the Linkam TS1400XY heating stage to melt inclusion studies. Cent. Eur. J. Geosci. 4, 208–218. https://doi.org/10.2478/S13533-011-0054-Y.

Esposito, R., Badescu, K., Steele-MacInnis, M., Cannatelli, C., De Vivo, B., Lima, A., Manning, C.E., 2018. Magmatic evolution of the Campi Flegrei and Procida volcanic fields, Italy, based on interpretation of data from well-constrained melt inclusions. Earth Sci. Rev. 185, 325–356.

Esposito, R., Redi, D., Danyushevsky, L.V., Gurenko, A., De Vivo, B., Manning, C.E., Frezzotti, M.L., 2023. Constraining the volatile evolution of mafic melts at Mt. Somma–Vesuvius, Italy, based on the composition of reheated melt inclusions and their olivine hosts. Eur. J. Mineral. 35 (6), 921–948.

Fedele, L., Tarzia, M., Belkin, H.E., De Vivo, B., Lima, A., Lowenstern, J.B., 2006. Magmatic-hydrothermal fluid interaction and mineralization in alkali-syenite nodules from the Breccia Museo pyroclastic deposit, Naples, Italy. In: De Vivo, B. (Ed.), Volcanism in the Campania Plain: Vesuvius, Campi Flegrei and Ignimbrites. Developments in Volcanology, 9. Elsevier, pp. 125–161.

Fedele, F.G., Giaccio, B., Isaia, R., Orsi, G., Carroll, M., Scaillet, B., 2007. The Campanian Ignimbrite factor: towards a reappraisal of the Middle to Upper Palaeolithic "transition". In: Grattan, J., Torrence, R. (Eds.), Living under the Shadow: The Cultural Impacts of Volcanic Eruptions. One World Archaeology Series, 53. Left Coast Press, Walnutt Creek, CA, USA, pp. 19–41.

Fedele, L., Scarpati, C., Lanphere, M., Melluso, L., Morra, V., Perrotta, A., Ricci, G., 2008. The Breccia Museo formation, Campi Flegrei, southern Italy: geochronology, chemostratigraphy and relationship with the Campanian Ignimbrite eruption. Bull. Volcanol. 70, 1189–1219. https://doi.org/10.1007/s00445-008-0197-y.

Fedele, L., Insinga, D., Calvert, A., Morra, V., Perrotta, A., Scarpati, C., 2011. $^{40}Ar/^{39}Ar$ dating of tuff vents in the Campi Flegrei caldera (southern Italy): toward a new chronostratigraphic reconstruction of the Holocene volcanic activity. Bull. Volcanol. 73, 1323–1336. https://doi.org/10.1007/s00445-011-0478-8.

Fedele, L., Scarpati, C., Sparice, D., Perrotta, A., Laiena, F., 2016. A chemostratigraphic study of the Campanian Ignimbrite eruption (Campi Flegrei, Italy): insights on magma chamber withdrawal and deposit accumulation as revealed by compositionally zoned stratigraphic and facies framework. J. Volcanol. Geotherm. Res. 324, 105–117. https://doi.org/10.1016/j.jvolgeores.2016.05.019.

Fettes, D., Desmons, J., 2007. Metamorphic rocks. A classification and glossary of terms. In: Recommendations of the International Union of Geological Sciences Subcommission on the Systematics of Metamorphic Rocks. Cambridge University Press, Cambridge, UK, p. 244.

Fournier, R.O., 1999. Hydrothermal processes related to movement of fluid from plastic into brittle rock in the magmatic-epithermal environment. Econ. Geol. 94, 1193–1211.

Freda, C., Gaeta, M., Giaccio, B., Marra, F., Palladino, D.M., Scarlato, P., Sottili, G., 2011. CO_2-driven large mafic explosive eruptions: the Pozzolane Rosse case study from the Colli Albani Volcanic District (Italy). Bull. Volcanol. 73, 241–256.

Frezzotti, M.L., Tecce, F., Casagli, A., 2012. Raman spectroscopy for fluid inclusion analysis. J. Geochem. Explor. 112, 1–20.

Fulignati, P., Marianelli, P., Santacroce, R., Sbrana, A., 2000. The skarn shell of the 1944 Vesuvius magma chamber. Genesis and P-T-X conditions from melt and fluid inclusion data. Eur. J. Mineral. 12, 1025–1039. https://doi.org/10.1127/0935-1221/2000/0012-1025.

Fulignati, P., Kamenetsky, V.S., Marianelli, P., Sbrana, A., Mernagh, T.P., 2001. Melt inclusion record of immiscibility between silicate, hydrosaline, and carbonate melts: applications to skarn genesis at Mount Vesuvius. Geology 29, 1043–1046. https://doi.org/10.1130/0091-7613(2001)029<1043.

Fulignati, P., Marianelli, M., Proto, M., Sbrana, A., 2004. Evidences for disruption of a crystallizing front in a magma chamber during caldera collapse: an example from the Breccia Museo unit (Campanian Ignimbrite eruption, Italy). J. Volcanol. Geotherm. Res. 133, 141–155. https://doi.org/10.1016/S0377-0273(03)00395-0.

Fulignati, P., Kamenetsky, V.S., Marianelli, P., Sbrana, A., 2005. Fluid inclusion evidence of second immiscibility within magmatic fluids (79 AD eruption of Mt. Vesuvius). Period. Mineral. 74, 43–54.

Gaeta, M., Di Rocco, T., Freda, C., 2009. Carbonate assimilation in open magmatic systems: the role of melt-bearing skarns and cumulate-forming processes. J. Petrol. 50, 361–385. https://doi.org/10.1093/petrology/egp002.

Gallo, R.I., Ort, M.H., Iacovino, K., Silleni, A., Smith, V.C., Giordano, G., Isaia, R., Boro, J., 2024. Reconciling complex stratigraphic frameworks reveals temporally and geographically variable depositional patterns of the Campanian Ignimbrite. Geosphere 19, 1–22. https://doi.org/10.1130/GES02651.1.

Gebauer, S.K., Schmitt, A.K., Pappalardo, L., Stockli, D.F., Lovera, O.M., 2014. Crystallization and eruption ages of Breccia Museo (Campi Flegrei caldera, Italy) plutonic clasts and their relation to the Campanian ignimbrite. Contrib. Mineral. Petrol. 167, 953. https://doi.org/10.1007/s00410-013-0953-7.

Giaccio, B., Hajdas, I., Isaia, R., Deino, A., Nomade, S., 2017. High-precision ^{14}C and $^{40}Ar/^{39}Ar$ dating of the Campanian Ignimbrite (Y-5) reconciles the time-scales of climatic-cultural processes at 40 ka. Sci. Rep. 7, 45940. https://doi.org/10.1038/srep45940.

Gilg, H.A., Lima, A., Somma, R., Belkin, H.E., De Vivo, B., Ayuso, R.A., 2001. Isotope geochemistry and fluid inclusion study of skarns from Vesuvius. Mineral. Petrol. 73, 145–176. https://doi.org/10.1007/s007100170015.

Hutsebaut, D., Vandenabeele, P., Moens, L., 2005. Evaluation of an accurate calibration and spectral standardization procedure for Raman spectroscopy. Analyst 130 (8), 1204–1214.

Iacono-Marziano, G., Gaillard, F., Scaillet, B., Pichavant, M., Chiodini, G., 2009. Role of non-mantle CO2 in the dynamics of volcano degassing: the Mount Vesuvius example. Geology 37 (4), 319–322.

Jolis, E.M., Troll, V.R., Harris, C., Freda, C., Gaeta, M., Orsi, G., Siebe, C., 2015. Skarn xenolith record crustal CO_2 liberation during Pompeii and Pollena Eruptions, Vesuvius Volcanic System, Central Italy. Chem. Geol. 415, 17–36. https://doi.org/10.1016/j.chemgeo.2015.09.003.

Knuever, M., Sulpizio, R., Mele, D., Costa, A., 2022. Magma–rock interactions: a review of their influence on magma rising processes with emphasis on short-timescale assimilation of carbonate rocks. Geol. Soc. Lond. Spec. Publ. https://doi.org/10.1144/sp520-2021-177. SP520-2021–177.

Knuever, M., Mele, D., Sulpizio, R., 2023a. Mineralization and skarn formation associated with alkaline magma chambers emplaced in a limestone basement: a review. Minerals 13, 1184. https://doi.org/10.3390/min13091184.

Knuever, M., Sulpizio, R., Mele, D., Pisello, A., Costa, A., Perugini, D., Vetere, F., 2023b. Decarbonation and clast dissolution timescales for short-term magma-carbonate interactions in the volcanic feeding system and their influence on eruptive dynamics: insights from experiments at atmospheric pressure. Chem. Geol., 121724 https://doi.org/10.1016/j.chemgeo.2023.121724.

Lentz, D., 1999. Carbonatite genesis: a reexamination of the role of intrusion-related pneumatholytic skarn processes in limestone melting. Geology 27, 335–338.

Lentz, D., 2017. Syntectic Reactions Involving Limestones and Limestone-Derived Carbonatitic Melts in the Generation of Some Peralkalic Magmas: Reflections on Reginald Daly's Insights 100 Years Later, Fall Meeting 2017, Abstract #V53A-03. American Geophysical Union.

Lima, A., Esposito, R., 2024. New views on Somma Vesuvius subvolcanic system and on mechanism that could increase eruption explosivity by a review and immiscibility in melt inclusions. J. Geochem. Explor. 256, 107348. https://doi.org/10.1016/j.gexplo.2023.107348.

Lima, A., De Vivo, B., Spera, F.J., Bodnar, R.J., Milia, A., Nunziata, C., Belkin, H.E., Cannatelli, C., 2009. Thermodynamic model for the uplift and deflation episodes (bradyseism) associated with magmatic-hydrothermal activity at the Campi Flegrei active volcanic center (Italy). Earth Sci. Rev. 97, 44–58. https://doi.org/10.1016/j.earscirev.2009.10.001.

Lima, A., Bodnar, R.J., De Vivo, B., Spera, F.J., Belkin, H.E., 2021. Interpretation of recent unrest events (bradyseism) at Campi Flegrei, Napoli (Italy): comparison of models based on cyclical hydrothermal events versus shallow magmatic intrusive events. Geofluids, 2000255. https://doi.org/10.1155/2021/2000255.

Lima, A., Bodnar, R.J., De Vivo, B., Spera, F.J., Belkin, H.E., 2025. The "breathing" Earth (la terra che respira) at Solfatara-Pisciarelli (Campi Flegrei, southern Italy) during 2005-2024: nature's way of attenuating the effects of bradyseism through gradual and episodic release of subsurface pressure. Am. Mineral. 110, 820–825. https://doi.org/10.2138/am-202-9516.

Lowe, J., Barton, N., Blockley, S., Ramsey, C.B., Cullen, V.L., Davies, W., Gamble, C., Grant, K., Hardiman, M., Housley, R., Lane, C.S., Lee, S., Lewis, M., MacLeod, A., Menzies, M., Muller, W., Pollard, M., Price, C., Roberts, A.P., Rohling, E.J., Satow, C., Smith, V.C., Stringer, C.B., Tomlinson, E.L., White, D., Albert, P., Arienzo, I., Barker, G., Boric, S., Carandente, A., Civetta, L., Ferrier, C., Guadelli, J.L., Karkanas, P., Koumouzelis, M., Muller, U.C., Orsi, G., Pross, J., Rosi, M., Shalamanov-Korobar, L., Sirakov, N., Tzedakis, P.C., 2012. Volcanic ash layers illuminate the resilience of Neanderthals and early modern humans to natural hazards. Proc. Natl. Acad. Sci. USA 109 (34), 13532–13537.

Lowenstern, J.B., 1993. Immiscibility between silicate melt, vapor and hydrosaline melt (~70-80 wt.% NaCl) in peralkaline rhyolites from Pantelleria, Italy. EOS 74, 670.

Lowenstern, J.B., 1994. Chlorine, fluid immiscibility, and degassing in peralkaline magmas from Pantelleria, Italy. Am. Mineral. 79, 353–369.

Meinert, L.D., 1998. Skarns and skarn deposits. Geosci. Can. 19, 145–162.

Meinert, L.D., Dipple, G.M., Nicolescu, S., 2005. World skarn deposits. In: Hedenquist, J. W., Thompson, J.F.H., Goldfarb, R.J., Richards, J.P. (Eds.), Economic Geology 100th Anniversary Volume. Society of Economic Geologists, Littleton, Colorado, USA, pp. 299–336. https://doi.org/10.5382/AV100.11.

Melluso, L., Morra, V., Perrotta, A., Scarpati, C., Adabbo, M., 1995. The eruption of the Breccia Museo (Campi Flegrei, Italy): fractional crystallization processes in a shallow, zoned magma chamber and implications for the eruptive dynamics. J. Volcanol. Geotherm. Res. 68, 325–339.

Milia, A., 2010. The stratigraphic signature of volcanism off Campi Flegrei (Bay of Naples, Italy). In: Groppelli, G., Viereck-Goette, L. (Eds.), Stratigraphy and Geology of Volcanic Areas, 464. Geological Society of America, pp. 155–170 of Special Paper.
Milia, A., Torrente, M.M., 1999. Tectonics and stratigraphic architecture of a pery-Tyrrhenian half-graben (Bay of Naples Italy). Tectonophysics 315, 297–314.
Milia, A., Torrente, M.M., 2011. The possible role of extensional faults in localizing magmatic activity: a crustal model for the Campanian Volcanic Zone (Eastern Tyrrhenian Sea, Italy). J. Geol. Soc. Lond. 168, 471–484. https://doi.org/10.1144/0016-76492010-121.
Milia, A., Torrente, M.M., 2020. Space-time evolution of an active volcanic field in an extensional region: the example of the Campania margin (eastern Tyrrhenian Sea). In: De Vivo, B., Belkin, H.E., Rolandi, G. (Eds.), Vesuvius, Campi Flegrei and Campanian Volcanism. Elsevier, pp. 297–320. ISBN: 978-0-12-816454-9.
Milia, A., Torrente, M.M., Russo, M., Zuppetta, A., 2003. Tectonics and crustal structure of the Campania continental margin: relationships with volcanism. Mineral. Petrol. 79, 33–47.
Nowaczyk, N.R., Arz, H.W., Frank, U., Kind, J., Plessen, B., 2012. Dynamics of the Laschamp geomagnetic excursion from Black Sea sediments. Earth Planet. Sci. Lett. 351, 54–69.
Orsi, G., 2022. Volcanic and deformation history of the Campi Flegrei Volcanic Field, Italy. In: Orsi, G., D'Antonio, M., Civetta, L. (Eds.), Campi Flegrei. A Restless Caldera in a Densely Populated Area. Active Volcanoes of the World. Springer, Berlin, Heidelberg, pp. 1–53. https://doi.org/10.1007/978-3-642-37060-1_1.
Orsi, G., Di Vito, M.A., Isaia, R., 2004. Volcanic hazard assessment at the restless Campi Flegrei caldera. Bull. Volcanol. 66, 514–530. https://doi.org/10.1007/s00445-003-0336-4.
Pabst, S., Wörner, G., Civetta, L., Tesoro, R., 2008. Magma chamber evolution prior to the Campanian ignimbrite and Neapolitan Yellow Tuff eruptions (Campi Flegrei, Italy). Bull. Volcanol. 70, 961–976. https://doi.org/10.1007/s00445-007-0180-z.
Pappalardo, L., Civetta, L., D'Antonio, M., Deino, A., Di Vito, M., Orsi, G., Carandente, A., de Vita, S., Isaia, R., Piochi, M., 1999. Chemical and Sr-isotopical evolution of the Phlegraean magmatic system before the Campanian Ignimbrite and the Neapolitan Yellow Tuff eruptions. J. Volcanol. Geotherm. Res. 91, 141–166.
Pascal, M.-L., Fonteilles, M., Boudouma, O., Principe, C., 2011. Qandilite from Vesuvius skarn ejecta: conditions of formation and miscibility gap in the ternary spinel-qandilite-magnesioferrite. Can. Mineral. 49, 459–485. https://doi.org/10.3749/canmin.49.2.459.
Peccerillo, A., 2017. Cenozoic volcanism in the Tyrrhenian Sea region. In: Advances in Volcanology. Springer Cham, p. 399. https://doi.org/10.1007/978-3-319-42491-0.
Perrotta, A., Luongo, G., Scarpati, C., Morra, V., 2006. The Campi Flegrei caldera boundary in the city of Naples. In: De Vivo, B. (Ed.), Volcanism in the Campania Plain: Vesuvius, Campi Flegrei and Ignimbrites, vol. 9. Elsevier, pp. 85–96. Series «Developments in Volcanology».
Petrosino, P., Arienzo, I., Mazzeo, F.C., Natale, J., Petrelli, M., Milia, A., Perugini, D., D'Antonio, M., 2019. The San Gregorio Magno lacustrine basin (Campania, southern Italy): improved characterization of the tephrostratigraphic markers based on trace elements and isotopic data. J. Quat. Sci. 34, 393–404. https://doi.org/10.1002/jqs.3107.
Pitzer, K.S., Sterner, S.M., 1994. Equations of state valid continuously from zero to extreme pressures for H_2O and CO_2. J. Chem. Phys. 101 (4), 3111–3116.
Pyle, D.M., Ricketts, G.D., Margari, V., van Andel, T.H., Sinitsyn, A.A., Praslov, N.D., Lisitsyn, S., 2006. Wide dispersal and deposition of distal tephra during the Pleistocene "Campanian Ignimbrite/Y5" eruption, Italy. Quat. Sci. Rev. 25, 2713–2728. https://doi.org/10.1016/j.quascirev.2006.06.008.
Remigi, S., Mancini, T., Ferrando, S., Frezzotti, M.L., 2021. Interlaboratory application of Raman CO_2 densimeter equations: experimental procedure and statistical analysis using bootstrapped confidence intervals. Appl. Spectrosc. 75 (7), 867–881. https://doi.org/10.1177/0003702820987601.
Remigi, S., Frezzotti, M.L., Rizzo, A.L., Esposito, R., Bodnar, R.J., Sandoval-Velasquez, A., Aiuppa, A., 2023. Spatially resolved CO_2 carbon stable isotope analyses at the microscale using Raman spectroscopy. Sci. Rep. 13 (1), 18561.
Roedder, E., 1979. Origin and significance of magmatic inclusions. Bull. Mineral. 102, 487–510.
Rolandi, G., Bellucci, F., Heizler, M., Belkin, H.E., De Vivo, B., 2003. Tectonic controls on the genesis of ignimbrites from the Campanian Volcanic Zone, southern Italy. Mineral. Petrol. 79, 3–31. https://doi.org/10.1007/s00710-003-0014-4.
Rolandi, G., De Natale, G., Kilburn, C.R.J., Troise, C., Somma, R., Di Lascio, M., Fedele, A., Rolandi, R., 2020a. The 39 ka Campanian Ignimbrite eruption: new data on source area in the Campanian Plain. In: De Vivo, B., Belkin, H.E., Rolandi, G. (Eds.), Vesuvius, Campi Flegrei and Campanian Volcanism. Elsevier, pp. 175–205. ISBN: 978-0-12-816454-9.
Rolandi, G., Di Lascio, M., Rolandi, R., 2020b. The Neapolitan Yellow Tuff eruption as the source of the Campi Flegrei caldera. In: De Vivo, B., Belkin, H.E., Rolandi, G. (Eds.), Vesuvius, Campi Flegrei and Campanian Volcanism. Elsevier, pp. 273–296. ISBN 9780128164549. https://doi.org/10.1016/B978-0-12-816454-9.00011-0.
Rose-Koga, E., Bouvier, A.-S., Gaetani, G., Wallace, P., Allison, C., Andrys, J., de la Torre, C.A., Barth, A., Bodnar, R., Gartner, A.B., 2021. Silicate melt inclusions in the new millennium: a review of recommended practices for preparation, analysis, and data presentation. Chem. Geol. 570, 120145.
Rosi, M., Sbrana, A., 1987. The Phlegrean Fields. C.N.R. Quaderni Ric. Sci. 114 (9), 175.
Salmoun, F., Dubessy, J., Garrabos, Y., Marsault-Herail, F., 1994. Raman spectra of H_2S along the liquid–vapour coexistence curve. J. Raman Spectrosc. 25 (4), 281–287.
Scarpati, C., Perrotta, A., 2016. Stratigraphy and physical parameters of the Plinian phase of the Campanian Ignimbrite eruption. Bull. Geol. Soc. Am. 128, 1147–1159. https://doi.org/10.1130/B31331.1.
Scarpati, C., Sparice, D., Perrotta, A., 2014. A crystal concentration method for calculating ignimbrite volume from distal ash-fall deposits and a reappraisal of the magnitude of the Campanian Ignimbrite. J. Volcanol. Geotherm. Res. 280, 67–75. https://doi.org/10.1016/j.jvolgeores.2014.05.009.
Scarpati, C., Sparice, D., Perrotta, A., 2020. Dynamics of large pyroclastic currents inferred by the internal architecture of the Campanian Ignimbrite. Sci. Rep. 10, 22230. https://doi.org/10.1038/s41598-020-79164-7.
Silleni, A., Giordano, G., Isaia, R., Ort, M.H., 2020. The magnitude of the 39.8 ka Campanian Ignimbrite eruption, Italy: method, uncertainties and errors. Front. Earth Sci. 8, 543399. https://doi.org/10.3389/feart.2020.543399.
Sillitoe, R.H., 2010. Porphyry copper systems. Econ. Geol. 105, 3–41. http://econgeol.geoscienceworld.org/content/105/1/3. https://doi.org/10.2113/gsecongeo.105.1.3.
Sottili, G., Taddeucci, J., Palladino, D.M., 2010. Constraints on magma-wall rock thermal interaction during explosive eruptions from textural analysis of cored bombs. J. Volcanol. Geotherm. Res. 192, 27–34. https://doi.org/10.1016/j.jvolgeores.2010.02.003.
Sterner, S.M., Pitzer, K.S., 1994. An equation of state for carbon dioxide valid from zero to extreme pressures. Contrib. Mineral. Petrol. 117, 362–374. https://doi.org/10.1007/BF00307271.
Tagirov, B., Schott, J., Harrichoury, J.-C., Salvi, S., 2002. Experimental study of aluminum speciation in fluoride-rich supercritical fluids. Geochim. Cosmochim. Acta 66, 2013–2024.
Tracy, R.J., Frost, B.R., 1991. Phase equilibria and thermobarometry of calcareous, ultramafic and mafic rocks, and iron formations. Rev. Mineral. Geochem. 26 (1), 207–289.
Troll, V.R., Hilton, D.R., Jolis, E.M., Chadwick, J.P., Blythe, L.S., Deegan, F.M., Schwarzkopf, L.M., Zimmer, M., 2012. Crustal CO2 liberation during the 2006 eruption and earthquake events at Merapi volcano, Indonesia. Geophys. Res. Lett. 39. https://doi.org/10.1029/2012GL051307.
Veksler, I.V., 2004. Liquid immiscibility and its role at the magmatic–hydrothermal transition: a summary of experimental studies. Chem. Geol. 210, 7–31. https://doi.org/10.1016/j.chemgeo.2004.06.002.
Veksler, I.V., Charlier, B., 2015. Silicate liquid immiscibility in layered intrusion. In: Charlier, B., et al. (Eds.), Layered Intrusion. Springer Geology. https://doi.org/10.1007/978-94-017-9652-1_5.
Wallace, P.J., Plank, T., Bodnar, R.J., Gaetani, G.A., Shea, T., 2021. Olivine-hosted melt inclusions: a microscopic perspective on a complex magmatic world. Annu. Rev. Earth Planet. Sci. 49, 465–494.
Whitley, S., Halama, R., Gertisser, R., Preece, K., Deegan, F.M., Troll, V.R., 2020. Magmatic and metasomatic effects of magma-carbonate interaction recorded in calc-silicate xenoliths from Merapi Volcano (Indonesia). J. Petrol. 61, egaa048. https://doi.org/10.1093/petrology/egaa048.